

RESEARCH

Open Access



Methyltransferase-like 7B participates in bladder cancer via ACSL3 m⁶A modification in a ferroptosis manner

Jiani He¹, Changming Dong^{2,3}, Xiandong Song^{2,3,4}, Zhongkai Qiu⁵, Hao Zhang^{2,3}, Yuanjun Jiang^{2,3}, Tao Liu^{2,3} and Xiaojun Man^{2,3*}

Abstract

Background Bladder cancer (BC) is a malignant tumor. Methyltransferase-like 7B (METTL7B) is a methyltransferase and its role in BC has not yet been revealed.

Method Stable METTL7B knockdown or overexpression were achieved by lentiviral transduction in SW780 and TCCSUP cell lines. Xenografts tumors were established via subcutaneous injection of stable transfectants in BALB/c mice.

Results A database search indicated that METTL7B was elevated in BC and it was validated in BC cell lines. METTL7B silencing suppressed cell proliferation and tumorigenesis in vitro and in vivo. Besides, METTL7B knockdown induced cell cycle arrest in G1 phase with a reduction in cyclin D1 (CCND1), CDK4, and CDK6 levels and an elevation in CDKN2D levels in cells. Considering that ferroptosis is emerging as a therapeutic target for cancer, and the possible relationship between METTL7B and antioxidant enzymes. We, here, examined that ectopic METTL7B expression abolished ferroptosis markers in cells raised by Erastin treatment, including the production of lipid ROS, the increased cellular iron and MDA content, the decreased gene expression of ACSL3, FANCD2, and FADS2, as well as the mitochondrial injury observed by electron microscopy. Mechanically, ectopic METTL7B expression promoted m⁶A modification on ACSL3 mRNA. Gain of functional experiment exhibited that METTL7B inhibited Erastin-induced ferroptosis via ACSL3. Overexpressed PLAGL2 is identified as a possible independent predictor in BC and bioinformatics predicted the potential binding sites between PLAGL2 and METTL7B promoter region. Dual luciferase and chromatin immunoprecipitation analysis provided evidence that PLAGL2 directly binds to METTL7B promoter region.

Conclusions METTL7B is involved in BC development and progression. METTL7B may mediate m⁶A modification on ACSL3 mRNA to negatively regulate ferroptosis in BC cells, which provides a potential therapeutic target for BC via ferroptosis.

Keywords Bladder cancer, METTL7B, m⁶A modification, ACSL3, Ferroptosis

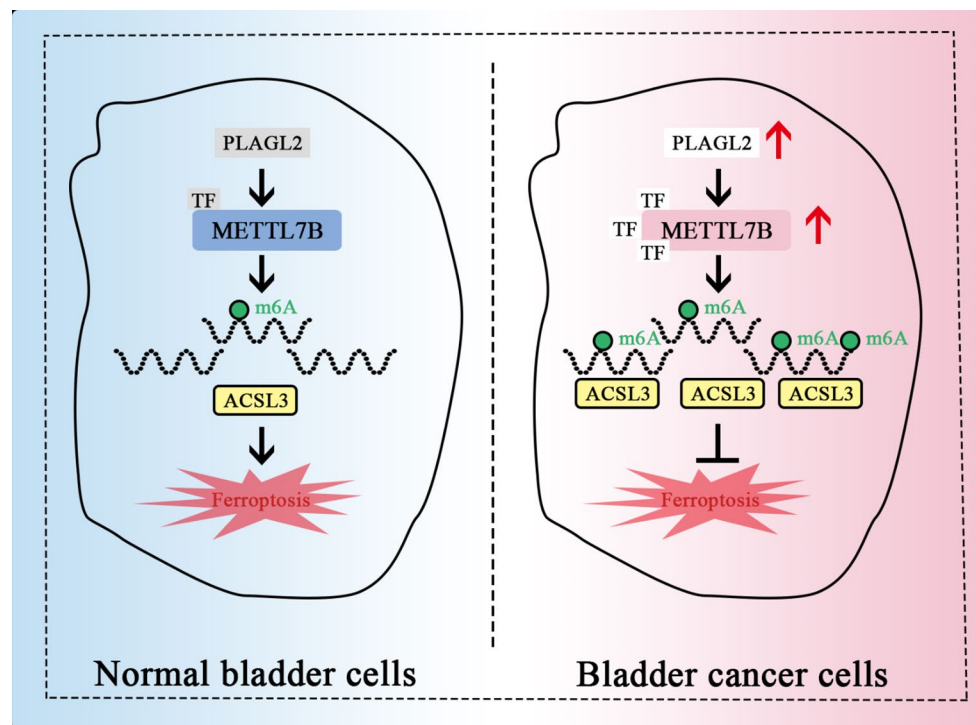
*Correspondence:

Xiaojun Man
manxj1983@163.com

Full list of author information is available at the end of the article



© The Author(s) 2025. **Open Access** This article is licensed under a Creative Commons Attribution-NonCommercial-NoDerivatives 4.0 International License, which permits any non-commercial use, sharing, distribution and reproduction in any medium or format, as long as you give appropriate credit to the original author(s) and the source, provide a link to the Creative Commons licence, and indicate if you modified the licensed material. You do not have permission under this licence to share adapted material derived from this article or parts of it. The images or other third party material in this article are included in the article's Creative Commons licence, unless indicated otherwise in a credit line to the material. If material is not included in the article's Creative Commons licence and your intended use is not permitted by statutory regulation or exceeds the permitted use, you will need to obtain permission directly from the copyright holder. To view a copy of this licence, visit <http://creativecommons.org/licenses/by-nc-nd/4.0/>.

Graphical Abstract**Background**

Bladder cancer (BC) is one of the commonest cancers of the genitourinary system and the ninth most common cancer in the world [1]. Globally, more than 430,000 people are diagnosed with BC each year, with nearly 170,000 deaths cases [2, 3]. BC can be classified as non-muscle invasive BC (NMIBC) and muscle-invasive BC (MIBC) according to the degree of muscle invasion. NMIBC, which makes up approximately three-quarters of BC, is usually treated by urethrectomy combined with intravesical bacillus Calmette-Guérin infusion. Although it frequently relapses, 10–30% of patients with NMIBC will progress to MIBC with decreased survival rate and frequent distant metastasis [4]. Metastasis is the leading cause of death in BC [5]. The 5-year survival rate for patients with BC is approximately 70%, compared to 5% for patients with metastases [1, 2]. Despite continuous improvements in surgical and chemotherapeutic approaches, there is an urgent need to identify new biomarkers and effective targets for the diagnosis and treatment of BC.

Methyltransferase-like (METTL) proteins are part of the superfamily of S-adenosylmethionine (SAM)-dependent enzymes that were characterized by the presence of methyltransferase-like domain [6]. They participate in chromatin organization and gene transcription modulation by transferring methyl group to nucleic acids,

proteins, small molecules, and so on [6] and have been implicated in various disease progression, including cancer [7]. Methyltransferase-like 7B (METTL7B) maps to chromosome 12. Previous studies have identified the role of METTL7B in metabolic and genetic diseases including non-alcoholic steatohepatitis lipid metabolism [8] and preeclampsia [9]. Moreover, the function of METTL7B in cancers has been discussed [10–12]. In terms of its role in bladder cancer, Campeanu et al. [13], identified the overexpressed METTL7B in BC in the TCGA database. However, its biological functions have not been revealed in vitro and in vivo, and the specific mechanisms by which it functions in BC are still not known.

Ferroptosis is a cell death program driven by redox and it is characterized by iron-dependent lipid peroxidation [14]. Iron is the essential executioner in ferroptosis, and the redox-iron leads to the accumulation of lipid-bases reactive oxygen species (ROS) which is the main cause of ferroptosis rather than cytosolic ROS. Although its physiological function is not yet clear [15], ferroptosis has been implicated in the involvement of cancer pathologic progression and is considered a promising cancer treatment because of the high iron content of cancer cells and their increased susceptibility to induce ferroptosis [16]. In BC, ferroptosis induction holds potent potential for cancer therapy [17]. GPX4 is the key regulator in ferroptosis, and METTL7B was implied to regulate the m⁶A

levels of GPX4 to promote its expression in lung adenocarcinoma [10]. Thus, it is interesting to explore whether METTL7B participates in ferroptosis regulation in BC.

In our work, we showed that METTL7B was overexpressed in BC and involved in tumor cell proliferation of BC. METTL7B facilitates ferroptosis progression by promoting m⁶A-based acyl CoA synthetase family 3 (ACSL3) mRNA levels, and ACSL3 negatively regulates ferroptosis sensitivity.

Methods

Cell culture and experimental treatments

Human BC cells lines (UMUC3, TCCSUP, T24, RT4, SW780, and 5637) and human immortalized uroepithelium cell line (SV-HUC-1) were purchased from iCell (Shanghai, China) and Procell (Wuhan, China). UM-UC-3 and TCCSUP cell lines were maintained in minimum essential medium (MEM) medium (Solarbio, Beijing, China). SV-HUC-1 cell line was maintained in F-12 K medium (Service biotechnology, Wuhan, China). 5637 cell line was maintained in RPMI-1640 medium (Solarbio, Beijing, China). SW780 cell line was maintained in L-15 medium (Solarbio, Beijing, China). RT4 and T24 cell lines were maintained in McCoy 5 A medium (Procell, Wuhan, China). All media were supplemented with 1% penicillin-streptomycin and 10% fetal bovine serum (FBS). Cells were incubated in a humidified air incubator at 37 °C with 5% CO₂. Cell lines with moderate METTL7B expression were screened by the RT-qPCR and western blot for further experiments.

To target METTL7B, lentivirus was produced from constructs containing non-targeting shRNA (shnc), shRNA targeting METTL7B, empty vector (nc), or METTL7B CDS (coding sequence). Cell lines were transfected with the lentivirus particles at a multiple of infection of 50 for 24 h. The stable transformants were selected with puromycin (Macklin, Shanghai, China) and validated by western blot and RT-qPCR. For RNA interference, cells were transfected with ACSL3 small interfering (si) RNA and non-targeting siRNA using Lipo3000 (Invitrogen, Carlsbad, CA, USA).

For Erastin treatment, cell lines were exposed to different concentrations of Erastin (Shanghai yuanye Bio-Technology Co., Ltd, Shanghai, China) for 24 h, which were referred from literatures [17, 18]. The cell inhibition analysis was performed afterward by the MTT assay, and the half-maximal inhibitory concentrations (IC₅₀) of Erastin in SW780 or TCCSUP cell lines were calculated. The stable transformants (with or without siRNA transfection) were stimulated with 3 μM in SW780 cells or 5 μM in TCCSUP cells for 24 h and then collected for further analysis.

Measurement of cell proliferation, colony formation, and cell cycle

The cell viability was measured by 3-[4,5-dimethylthiazol-2-yl]-2,5 diphenyltetrazolium bromide (MTT). Cells were cultured in 96-well plates at a density of 5×10^3 /well with designated treatments. After that, the medium was replaced with 50 μL MTT solution (KeyGEN, Nanjing, China) and cultured for 4 h. MTT solution was then replaced by 150 μL dimethyl sulfoxide (DMSO) (KeyGEN, Nanjing, China) to dissolve MTT formazan. The absorbance was measured at 490 nm by a microplate reader. Cells were seeded into cell culture dishes at a density of 500 cells/dish. Two weeks after inoculation, the clones were fixed with paraformaldehyde and stained with Giemsa dye solution (KeyGen Biotech., Nanjing, China), and then the number of cell colonies was counted and photographed under a microscope to calculate the colony formation rate. After designated treatment, cells were collected and fixed in 70% ethanol overnight at 4 °C. Cells were stained with propidium iodide (PI) and treated with RNase A (Beyotime, Shanghai, China). Cell cycle curves were analyzed using flow cytometry.

Lipid reactive oxygen species (ROS), malondialdehyde (MDA), and iron content analysis

Lipid ROS production in cells was detected by probing with C11-BODIPY^{581/591} (Maokang, Shanghai, China) dye at the final concentration of 2 μM and incubated for 20 min before subjecting to flow cytometry. Cell lysates were assayed for MDA (Beyotime, Shanghai, China), iron (Leagene, Beijing, China), and Ferrous Ion content (Solarbio, Beijing, China) via commercial kits according to kit instructions.

Immunohistochemistry (IHC) and electron microscopy

For IHC of xenograft tumors, the slides were stained with primary antibodies against METTL7B (Proteintech Group, Inc., Wuhan, China), Ki67 (Affinity, Changzhou, China) and ACSL3 (ABclonal, Wuhan, China) overnight at 4 °C, followed by secondary antibody (Thermo Scientific, Pittsburgh, PA, USA) incubation for 1 h at 37 °C. Thereafter, the slides were developed with 3,3'-diaminobenzidine tetrahydrochloride (DAB), re-stained with hematoxylin, and photographed under the fluorescence microscope (Olympus, Tokyo, Japan). Electron microscopy was used to examine mitochondrial morphology as previously described [19].

Western blot

Total cellular proteins were lysed on ice for 5 min in radioimmune precipitation assay (RIPA) buffer (Solarbio, Beijing, China) containing phenylmethanesulfonyl fluoride (PMSF) (Solarbio, Beijing, China). Protein concentration was detected as described in BCA kit (Solarbio,

Beijing, China) instructions. Proteins were separated by sodium dodecyl sulfate polyacrylamide gel electrophoresis (SDS-PAGE) (Solarbio, Beijing, China) and then transferred to polyvinylidene fluoride (PVDF) (Millipore, Billerica, MA, USA) membranes. After blocking, the membranes were incubated with appropriate diluted primary antibodies overnight at 4 °C: METTL7B (ABclonal, Wuhan, China, A7200), ACSL3 (Proteintech Group, Inc., Wuhan, China, 20710-1-AP), PLAGL2 (Proteintech Group, Inc., Wuhan, China, 11540-1-AP), CDKN2D (ABclonal, Wuhan, China, A6556), CCND1 (ABclonal, Wuhan, China, A19038), CDK6 (ABclonal, Wuhan, China, A0106), CDK4 (ABclonal, Wuhan, China, A23522), GAPDH (Proteintech Group, Inc., Wuhan, China, 60004-1-Ig) (loading control) and then corresponding secondary antibodies horseradish peroxidase (HRP)-conjugated goat anti-rabbit to IgG or HRP conjugated goat anti-mouse to IgG (Solarbio, Beijing, China) for 60 min at 37 °C. Enhanced chemiluminescence (ECL) kit (Solarbio, Beijing, China) was used to visualize the protein bands.

Reverse transcription quantitative polymerase chain reaction (RT-qPCR)

Total cellular RNAs were isolated using TRIpure (Biotek, Beijing, China) based on standard instruction of manufacture. Afterward, the obtained RNA was used for cDNA synthesis by BeyoRT II M-MLV reverse transcriptase (Beyotime, Shanghai, China). Gene expression was quantified using SYBR Green (Solarbio, Beijing, China) on Exicycler 96 (Bioneer, Daejeon, Korea) and calculated with the $2^{-\Delta\Delta C_t}$ method. The primer sequences for the genes were as follows: ACSL3 forward: 5'-GAGTGGGAGCACCATTAG-3' and reverse: 5'-AGAGCCACCTTTGTCCAT-3'. CDK4 forward: 5'-AAGTGGTGGAACAGTCAAG-3' and reverse: 5'-AGCCCAATCAGGTCAA-3'. CDKN2D forward: 5'-ATGCTGCTGGAGGAGGTTC-3' and reverse: 5'-TTGAGGGCGTTCGGGATG-3'. FADS2 forward: 5'-GAAATACCTGCCCTACAAT-3' and reverse: 5'-CCCAGTTCTTATGGACGA-3'. FANCD2 forward: 5'-TGTCTTGTGAGCGTCTG-3' and reverse: 5'-GCATGATCTTGGTGGTG-3'. METTL7B forward: 5'-TTTCAGTTCTACCCACCG-3' and reverse: 5'-CACCACAAACCGTCTCAT-3'. PLAGL2 forward: 5'-AGTCAAGTGAAGTGCCAATG-3' and reverse: 5'-CTTGCGGTGAAACATCTTAT-3'. CCND1 forward: 5'-GCGAGGAACAGAAGTGCG-3' and reverse: 5'-GGAGTTGTCGGTGTAGATGC-3'. CDK6 forward: 5'-ACGTGTGTCAGGTTGTTT-3' and reverse: 5'-CTTTATGGTTTCAGTGGG-3'. GAPDH forward: 5'-GACCTGACCTGCGTCTAG-3' and reverse: 5'-AGGAGTGGGTGTCGTGT-3'.

Methylated RNA immunoprecipitation (MeRIP)-RT-qPCR

m⁶A modification on ACSL3 was validated by MeRIP-RT-qPCR assay referred to [20] using m⁶A Transcriptome Profiling Kit (RiboBio Co. Ltd., Guangzhou, China). Briefly, 18 µg of total extracted RNA was sheared into fragments using RNA Fragmentation Buffer. Anti-m⁶A antibody or IgG were immobilized on magnetic beads A/G in m⁶A IP buffer. Roughly one-tenth of the fragment was reserved as the input control, and the remaining was incubated with m⁶A-conjugated beads and rotated for 2 h at 4 °C. m⁶A-containing RNA fragments were eluted from the beads and then purification was performed for further analysis by RT-qPCR. Relative m⁶A enrichment was calculated by normalizing it to the input.

Dual luciferase reporter

To evaluate the regulation of PLAGL2 on METTL7B promoter activity, luciferase promoter reporter gene constructs of different lengths of METTL7B were created and cloned in pGL3-basic vector. SW780 cells were co-transfected with pGL3-METTL7B promoter construct, renilla luciferase control vector, and PLAGL2 overexpression plasmid (or empty vector) using a Lipofectamine 3000 kit. After 48 h transfection, the luciferase activity was measured using the dual luciferase reporter assay system (KeyGen Biotech., Nanjing, China).

Chromatin immunoprecipitation (ChIP) assay

Cellular proteins were cross-linked with chromatin using 1% formaldehyde for 10 min at room temperature and quenched by glycine for 5 min. Then cells were washed twice in pre-cooling PBS, dissociated in ChIP lysis buffer, and sonicated to 500–1000 bp. Cell lysates were incubated over night at 4 °C with antibodies or IgG control followed by capture with protein A beads for 1–2 h. After washing, the immunoprecipitated DNA was eluted and uncrosslinked for further PCR analysis. Three pairs of oligonucleotide primers covering METTL7B were used to analyze the PLAGL2-putative binding site in METTL7B: primer 1: 5'-TGTCCCCAGCATTCACCACT-3' and reverse: 5'-ACAGCCCCACAAGCTCTTCA-3'. METTL7B primer 2: 5'-AACTTACCCCATTCCCCA CA-3' and reverse: 5'-CGTCCTCAGGTCAGGCACT T-3'. METTL7B primer 3: 5'-TTGTCCCCTCCAAATC TCA-3' and reverse: 5'-GGAAGCATGGCACCAGTA T-3'.

Xenograft mouse model

BALB/c male nude mice were obtained from Cavens lab (Changzhou, China). All experiments were approved by the Ethics Committee of China Medical University. The procedures were conducted as previously described [21]. A total of 1×10^6 SW780 cells containing METTL7B knockdown or negative control were subcutaneously

injected into mice. When tumor size reached 50 mm³, the mice received a dose (15 mg/kg) of Erastin (intra-peritoneal injection for every two days). Tumor volume was measured every 4 days, and mice were sacrificed 20 days after tumor cell injection.

Statistical analysis

GraphPad Prism version 8 (GraphPad Software Inc., San Diego, CA, USA) was used to conduct statistical analysis and generate bar graphs and plots. Student's t-test, one-way analyses of variance (ANOVA), or two-way ANOVA was utilized to compare group differences. All data were presented as mean ± standard deviation with at least three independent experiments. *P* values of <0.05 were regarded as significance.

Results

Expression of METTL7B in bladder cancer

Studies had revealed that METTL family participated in multiple biological functions and functions in human diseases, including cancer [22]. Through the GEPIA database, we identified 4 differentially expressed genes (DEGs) from METTL family (Fig. 1A), including METTL7B, METTL1 (known function in BC), METTL7A (unresolved precise targets and functions), and METTL24 (newly identified methyltransferase). Combined with their function and investigation in BC or other diseases, METTL7B draws our attention. The up-regulated METTL7B expression in BC tissues was validated in GEPIA (Fig. 1B) and TNMplot (Fig. 1C) database. In addition, pan-cancer analysis showed that METTL7B was up-regulated in multiple types of cancer (Fig. 1D). Results demonstrated that the METTL7B mRNA and protein (Fig. 1E-F) expression levels were significantly increased in the majority of BC cell lines including UMUC3, TCCSUP, RT4, and SW780, when compare to normal uroepithelial SV-HUC-1 cells. Based on the results, the higher expression cell lines, SW780 and TCCSUP, were employed for subsequent experiments.

Proliferative effect of METTL7B in bladder cancer cells

To explore the role of METTL7B in BC, we silenced or overexpressed the METTL7B expression in SW780 and TCCSUP cell lines, and the transfection efficiency was validated (Fig. 2A-B). As results showed that silenced METTL7B exhibited a marked decrease in cell viability and clone formation of SW780 and TCCSUP cells (Fig. 2C, E). Meanwhile, the cell cycle of SW780 and TCCSUP was arrested in G1 phase in response to METTL7B knockdown (Fig. 2G). In addition, increasing METTL7B levels promoted cell viability, colony formation, and cell cycle progression (Fig. 2D, F, H). Consistent with the above results, the increased expression of cell cycle-related genes, including CCND1, CDK4, CDK6, and

CDKN2D, was observed in SW780 and TCCSUP cell with METTL7B overexpression (Fig. 2J and supplementary Fig. 1), and the opposite results were observed in METTL7B knockdown cells (Fig. 2I and supplementary Fig. 1).

METTL7B negatively regulated Erastin-induced ferroptosis in bladder cancer cells

Increasingly evidence has highlighted the importance of ferroptosis in tumorigenesis and development [15]. We, therefore, asked whether METTL7B contributed to ferroptosis sensitivity in BC cells. Cells were exposed to indicated concentrations of Erastin for 24 h. MTT results showed that the depletion of METTL7B aggravated the ferroptosis sensitivity of SW780 and TCCSUP cells to Erastin and decreased the IC50 value compared to the control cells (Fig. 3A). Reversely, METTL7B overexpression promoted ferroptosis resistance and the corresponding IC50 value in cells (Fig. 3B). Subsequently, 3 μM Erastin for SW780 and 5 μM Erastin for TCCSUP were chosen for the following experiment, as they were close to their IC50 values. To further unravel the mechanism of METTL7B against ferroptosis, the ferroptosis-associated indicators and genes were examined. Intracellular lipid ROS production detected by C11-BODIPY 581/591 probe showed that lipid ROS accumulated in METTL7B silencing SW780 and TCCSUP cells with Erastin treatment (Fig. 3C), but abolished in cells transduced with METTL7B overexpression (Fig. 3D). A similar trends of MDA (Fig. 3E) and cellular iron content (Fig. 3F) were also observed in indicated SW780 and TCCSUP cells in response to Erastin treatment. Evidence indicated that ferroptotic cells displayed smaller mitochondrial and the reduction or vanishment of mitochondrial cristae [23]. Using transmission electron microscopy, the mitochondrial were swollen and round in cells upon Erastin stimulation and these phenomena were aggravated in METTL7B knockdown cells (with weak or even bright matrix) (Fig. 3G) or alleviated in METTL7B overexpressed cells (Fig. 3G). These results indicated a possible involvement of METTL7B in Erastin-induced ferroptosis regulation.

METTL7B promoted the m⁶A modification on ACSL3 mRNA and negatively regulated Erastin-induced ferroptosis via ACSL3

The fate of METTL7B is to catalyze m⁶A formation on target mRNA. To identify METTL7B acting on ferroptosis-related genes, the mRNA levels of ACSL3, FANCD2, and FADS2 were examined. These factors were identified as the novel ferroptosis-related prognostic factor in BC [24]. As results showed that these genes were decreased in METTL7B knockdown cells and increased in METTL7B overexpression cells (Fig. 4A). Among

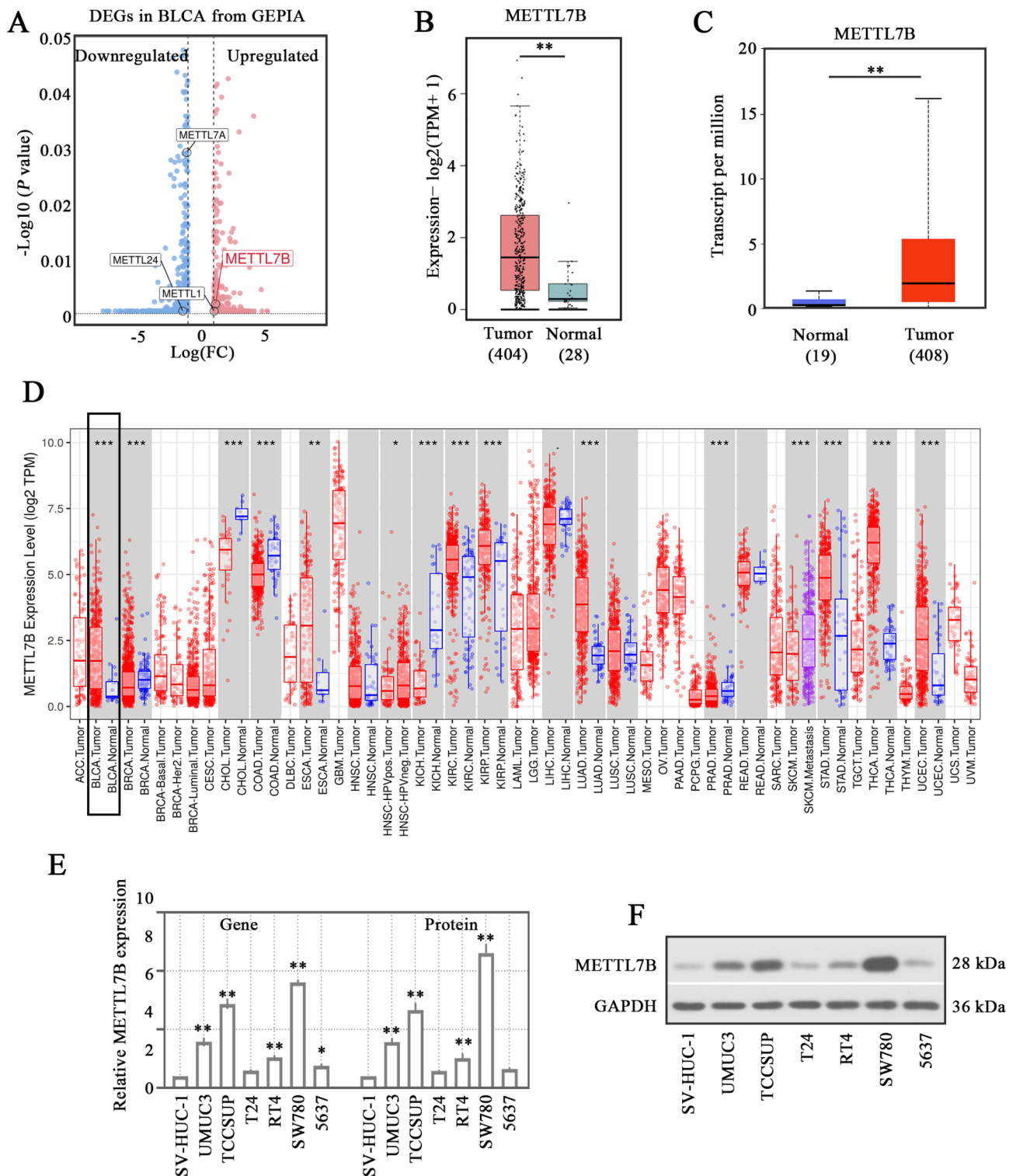


Fig. 1 Expression of METTL7B in bladder cancer. **A**) Volcano plots showing differential gene expression in bladder cancer from GEPIA database. The black circle represented the differentially expressed gene in METTL family, including METTL7B, METTL1, METTL24, and METTL7A. **B-C**) Expression of METTL7B in bladder cancer from GEPIA (**B**) and UALCAN database (**C**). **D**) The pan-cancer expression pattern of METTL7B in tumor and non-tumor tissues from TIMER database. **E-F**) METTL7B mRNA (**E**) and protein (**F**) expression in normal uroepithelial SV-HUC-1 cells and bladder cancer cell lines. GEPIA: gene expression profiling interactive analysis. METTL: methyltransferase-like. UALCAN: University of Alabama at Birmingham Cancer Data Analysis Portal. TIMER: Tumor Immune Estimation Resource. **P* < 0.05, ***P* < 0.01 versus SV-HUC-1

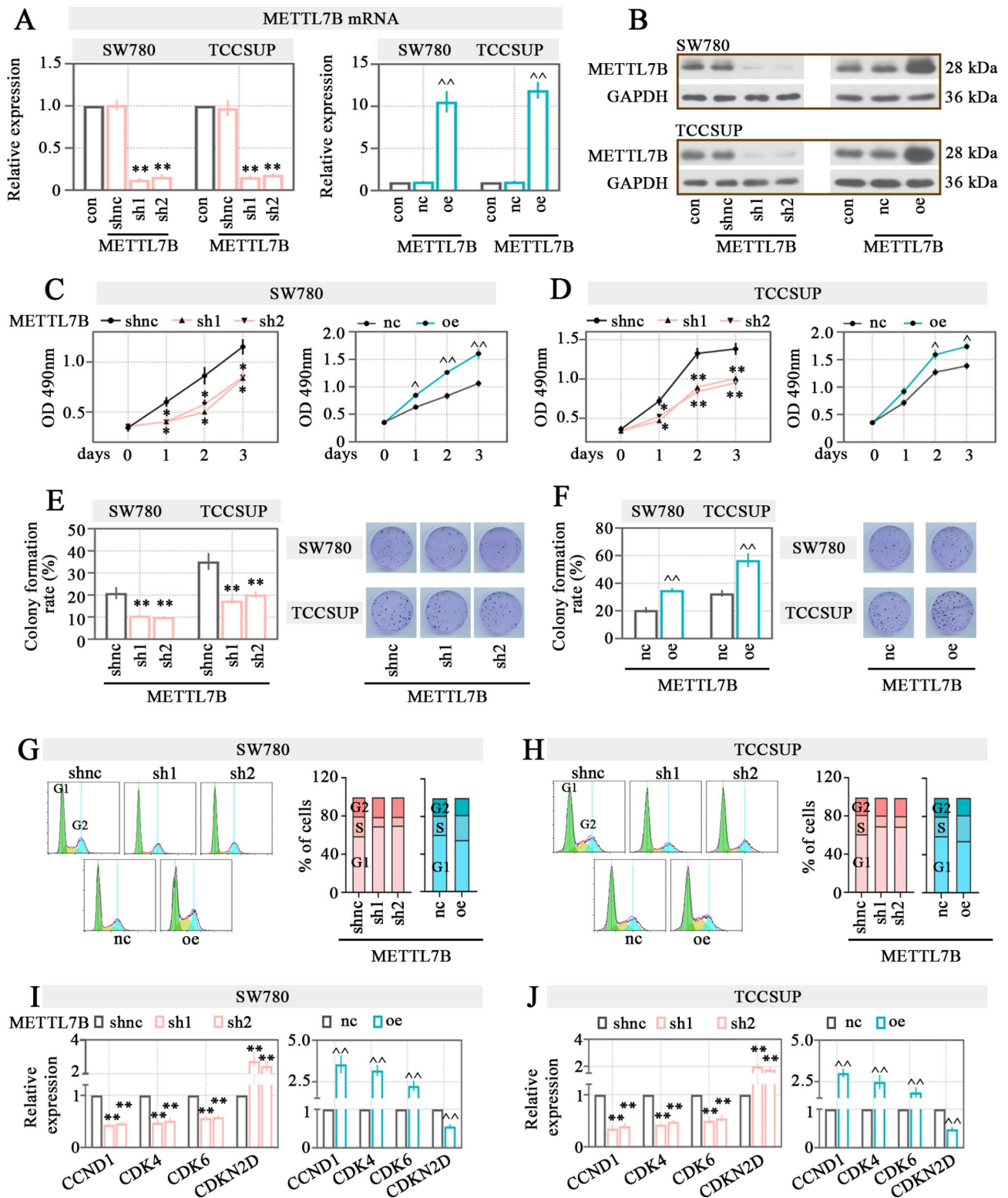


Fig. 2 Proliferative effect of METTL7B in bladder cancer cells. **A-B** Efficiencies of METTL7B knockdown or overexpression were validated by RT-qPCR (**A**) and western blot (**B**) in SW780 and TCCSUP cell lines. **C-D** Proliferation of SW780 (**C**) and TCCSUP (**D**) cells with METTL7B knockdown or overexpression was measured by MTT assay. **E-F** Colony formation assay of SW780(**E**) and TCCSUP (**F**) cells with METTL7B knockdown or overexpression. **G-H** Cell cycle of SW780 (**G**) and TCCSUP (**H**) cells with METTL7B knockdown or overexpression was measured by propidium iodide staining using flow cytometry. **I-J** RT-qPCR measurement of cell cycle-related genes such as CCND1, CDKN2D, CDK4, and CDK6. METTL: methyltransferase-like. CCND1: cyclin D1. CDKN2D: cyclin dependent kinase inhibitor 2D. CDK: cyclin Dependent kinase. Con: control. shnc: negative control short hairpin RNA. sh1/2: short hairpin RNA 1/2 against METTL7B. nc: empty vector plasmid. oe: METTL7B overexpression plasmid. **P*<0.05, ***P*<0.01 versus shnc. ^*P*<0.05, ^^*P*<0.01 versus nc

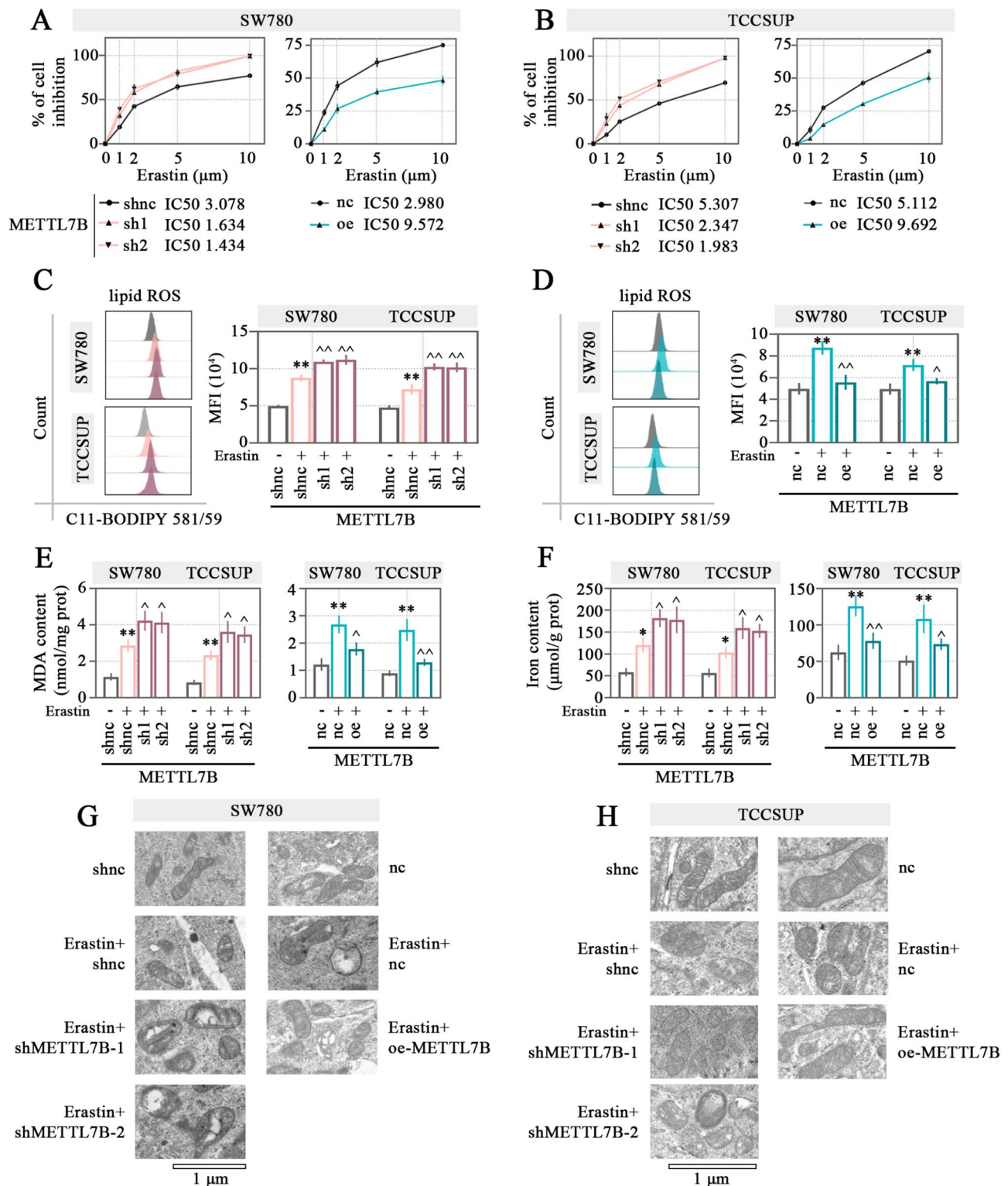


Fig. 3 METTL7B negatively regulated Erastin-induced ferroptosis in bladder cancer cells. **A-B** Indicated SW780 (**A**) or TCCSUP (**B**) cells were treated with Erastin with different concentrations for 24 h, and the cell viability was measured by MTT assay. **C-D** Lipid ROS production in SW780 (**C**) or TCCSUP (**D**) with METTL7B knockdown or overexpression was measured by C11-BODIPY 581/591 staining using flow cytometry. **E-F** MDA (**E**) and total cellular iron content (**F**) in indicated cells were detected using corresponding commercial kits. **G-H** Representative images of cell mitochondrial ultrastructure captured by Transmission electron microscopy. Scale bar = 1 μm . MTT: 3-(4, 5-dimethylthiazol-2-yl)-2, 5 diphenyltetrazolium bromide. MDA: malondialdehyde. shnc: negative control short hairpin RNA. sh1/2: short hairpin RNA 1/2 against METTL7B. nc: empty vector plasmid. oe: METTL7B overexpression plasmid. * $P < 0.05$, ** $P < 0.01$ versus shnc or nc. ^ $P < 0.05$, ^^ $P < 0.01$ versus Erastin + shnc or Erastin + nc

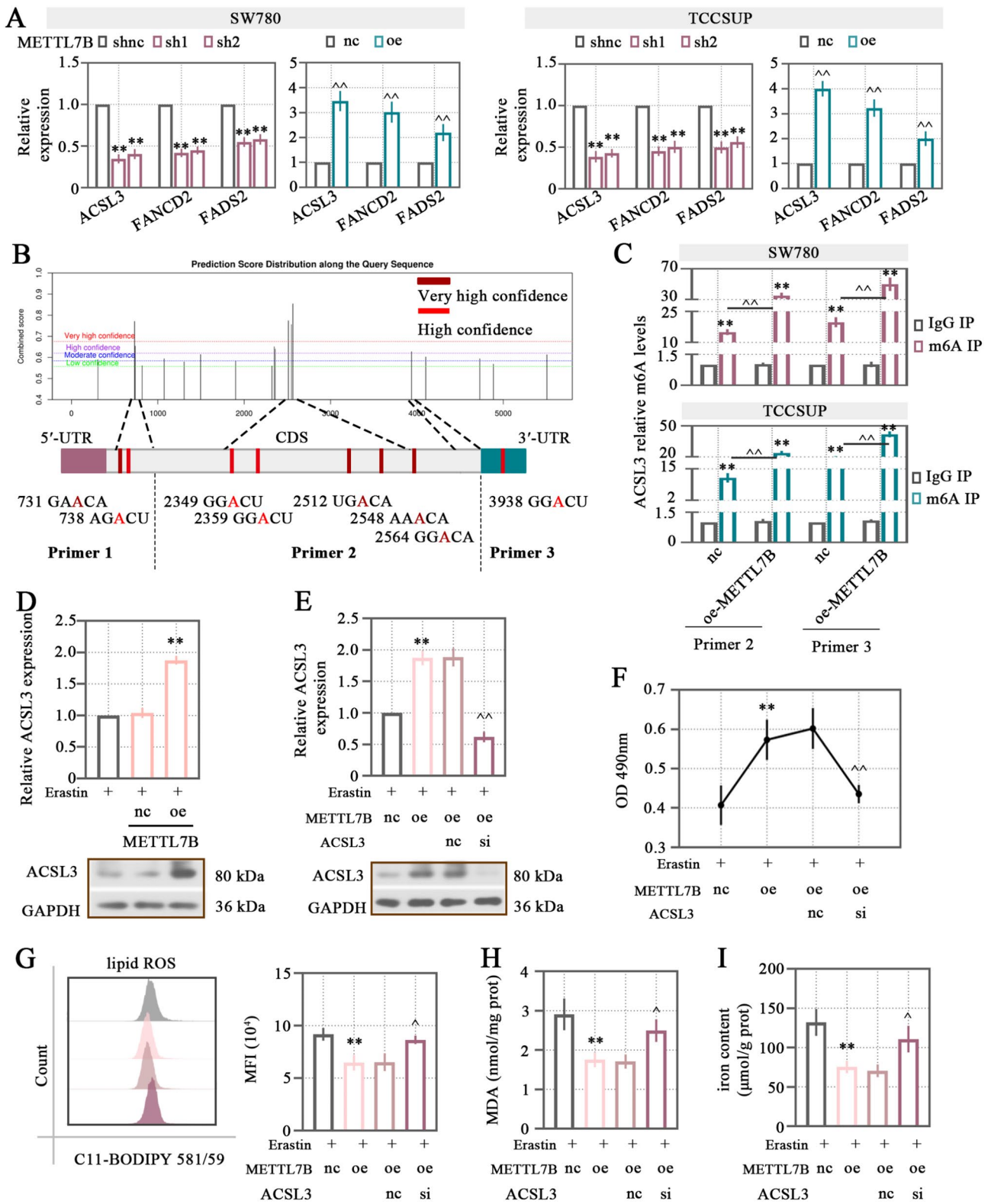


Fig. 4 (See legend on next page.)

(See figure on previous page.)

Fig. 4 METTL7B promoted the m⁶A modification on ACSL3 mRNA and negatively regulated Erastin-induced ferroptosis via ACSL3. **(A)** RT-qPCR measurement of ferroptosis-related regulators SW780 and TCCSUP cells, including ACSL3, FANCD2, and FADS2. ***P* < 0.01 versus shnc. ^^*P* < 0.01 versus nc. **(B)** Bioinformatics site SRAMP predicted potential m⁶A methylation sites in the sequence of ACSL3. **(C)** Detection of m⁶A levels among potential binding sites of ACSL3 by m⁶A-IP-RT-qPCR in SW780 and TCCSUP cells. ***P* < 0.01 versus IgG IP. ^^*P* < 0.01 versus IgG IP (nc). **(D)** The mRNA and protein expression levels of ACSL3 in Erastin-treated SW780 cells with METTL7B overexpression. **(E)** The mRNA and protein expression levels of ACSL3 in Erastin-treated SW780 cells with METTL7B overexpression and/or ACSL3 knockdown. **(F)** Proliferation of SW780 cells with METTL7B overexpression and/or ACSL3 knockdown was measured by MTT assay. **(G)** Lipid ROS production in SW780 cells with METTL7B overexpression and/or ACSL3 knockdown was measured by C11-BODIPY 581/591 staining using flow cytometry. **(H-I)** MDA **(H)** and intracellular iron content **(I)** in SW780 cells with METTL7B overexpression and/or ACSL3 knockdown were detected using corresponding commercial kits. ***P* < 0.01 versus Erastin + METTL7B nc. ^^*P* < 0.01 versus Erastin + METTL7B oe + nc. shnc: negative control short hairpin RNA. sh1/2: short hairpin RNA 1/2 against METTL7B. nc: empty vector plasmid or small interfering RNA negative control. si: small interfering. oe: METTL7B overexpression plasmid. ACSL3, acyl-coA synthetase long chain family member 3. FANCD2, FA complementation group D2. FADS2: fatty acid desaturase 2. METTL: methyltransferase-like. MTT: 3-(4, 5-dimethylthiazol-2-yl)-2, 5 diphenyltetrazolium bromide. MDA: malondialdehyde

these candidates, ACSL3 showed remarkable changes. Using the online tool SRAMP (<http://www.cuilab.cn/sramp>) (Fig. 4B), various m⁶A modification sites on ACSL3 genome were shown. Primers were designed for the probe for m⁶A modification sites at these 8 sites in ACSL3 (Fig. 4B). From the MeRIP assay, ACSL3 was enriched in m⁶A precipitated fraction and METTL7B overexpression promoted m⁶A-methylated ACSL3 mRNA levels in cells (Fig. 4C). Next, we examined whether METTL7B participates in ferroptosis via ACSL3. As results showed that ACSL3 mRNA and protein levels were upregulated in METTL7B overexpressed cells upon Erastin stimulation (Fig. 4D). A rescue experiment was subsequently performed. We found that ACSL3 knockdown was sufficient to rescue the increased ACSL3 levels upon METTL7B overexpression (Fig. 4E), and the increased cell viability of cells (Fig. 4F). Moreover, ACSL3 knockdown increased the lipid ROS (Fig. 4G), MDA (Fig. 4H), and iron content (Fig. 4I) in cells induced by METTL7B overexpression and Erastin stimulation, indicating that METTL7B might be participating in ferroptosis through ACSL3.

METTL7B inhibited tumor growth and ferroptosis in xenograft tumor model induced by Erastin

The effect of METTL7B was further examined in a mouse xenograft model. As shown in Fig. 5A, the tumor growth was restrained in mice following METTL7B inhibition in SW780 cells. Combined with Erastin treatment, the tumor volume decreased in METTL7B knockdown group relative to the negative control group, although falling short of significance (Fig. 5A). As expected, the tumor weight showed a similar trend as the tumor volume results (Fig. 5B). IHC results exhibited a lower Ki67, METTL7B, and ACSL3 levels in excised tumor from the METTL7B silencing group, while excised tumor from Erastin plus METTL7B inhibition group showed an obvious decrease in these protein levels (Fig. 5C). In addition, the reduced protein expression of ACSL3 (Fig. 5D) and ferrous iron content (Fig. 5E) were confirmed upon METTL7B knockdown, while a slight reduction of these levels was observed in tumor tissue of mice in combination with Erastin treatment. Similarly, the MDA content

was increased in tumor with METTL7B knockdown, and Erastin-treated mice had higher levels compared to the vehicle treated-mice (Fig. 5F). The results indicated that METTL7B might play a role in the regulation of ferroptosis, as its effect was not further enhanced by Erastin.

Involvement of PLAGL2 in METTL7B transcriptional regulation

Next, we sought to determine the potential upstream regulators of METTL7B. PLAGL2, a zinc-finger transcription factor, is involved in pathogenesis of multiple cancers. Recently, PLAGL2 was identified to correlate with the pathological features and prognosis in BC tissues [25]. The database survey revealed the higher PLAGL2 expression in BC tissues and a positive correlation exists between PLAGL2 and METTL7B (Fig. 6A-B). Additionally, a publicly available database predicts the possible binding site of PLAGL2 and METTL7B. RT-qPCR and Western blot (Fig. 6D) validated the loss or gain of METTL7B expression upon PLAGL2 silencing or overexpression (the transfection efficiency was shown in Fig. 6C). According to predict results, three truncated METTL7B reporter plasmids were constructed. The dual luciferase results revealed that PLAGL2 overexpression significantly promoted the luciferase activity of all reporter plasmids (Fig. 6E). Therefore, we designed the PCR primers to amplify the three putative binding sites on the METTL7B DNA sequences. As results indicated that the PLAGL2 binding motif located in -461~-451 bp (primer 2) and -262~-253 bp (primer 3) on the METTL7B promoter region (Fig. 6F).

Discussion

In our study, we proved the function of METTL7B in BC progression and development both in vitro and in vivo. On the one hand, METTL7B was overexpressed in BC and its upregulation promoted cell proliferation. On the other hand, METTL7B is involved in the ferroptosis progression of BC cells. Mechanically, METTL7B increased ACSL3 expression via m⁶A modification to negatively modulate the ferroptosis sensitivity of BC cells. METTL7B may be a new, potential therapeutic target for BC.

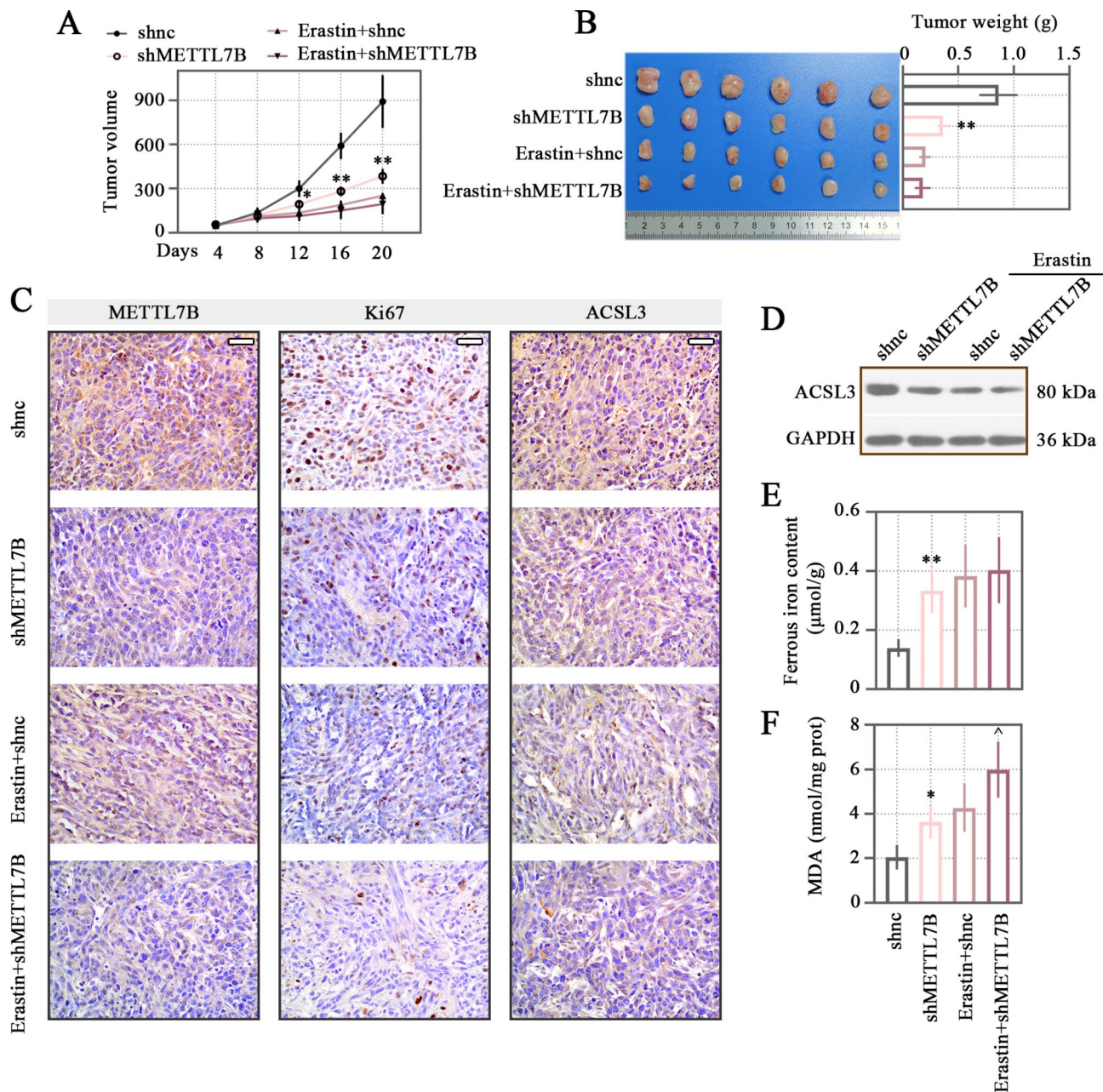


Fig. 5 METTL7B inhibited tumor growth and ferroptosis in xenograft tumor model induced by Erastin. **(A)** Tumor growth curves of xenograft tumors derived from SW780 cells with METTL7B knockdown. **(B)** Representative images of xenograft tumors (left panel) and tumor weights (right panel) of xenograft from SW780 cells in nude mice. **(C)** Immunohistochemical analysis of METTL7B, Ki67, and ACSL3 in SW780 xenograft tumors. Scale bar = 50 μ m. **(D)** The protein expression levels of ACSL3 in tumor. **(E-F)** Ferrous iron **(E)** and MDA **(F)** content in SW780 xenograft tumors was detected using corresponding commercial kits. METTL7B: methyltransferase-like 7B. ACSL3, acyl-coA synthetase long chain family member 3. MDA: malondialdehyde. shnc: negative control short hairpin RNA. shMETTL7B: short hairpin RNA against METTL7B. * $P < 0.05$, ** $P < 0.01$ versus shnc. ^ $P < 0.05$ versus Erastin + shnc

METTL7B was first identified to be a Golgi-related methyltransferase [26] and reported to function in cancers. But, its role in cancer was controversial: on the one hand, METTL7B was upregulated and promoted cell malignant behavior in lung adenocarcinoma [10] and glioma [11], whereas on the other hand, increased METTL7B was suggested to exert suppressing effect in breast cancer [12]. In our work, we revealed that METTLB was

upregulated in multiple BC cell lines, and its upregulation exacerbated cell proliferation and colony formation. Besides, METTL7B knockdown induced a cell cycle arrest in G0/G1 phase. CCNDK1 is a cell cycle regulator, and its abnormal expression was correlated with BC development [27]. CCDN1 is the regulatory subunit of CDK4 and CDK6, which interact with them and inhibit their activity [28]. All of them are responsible for the G1

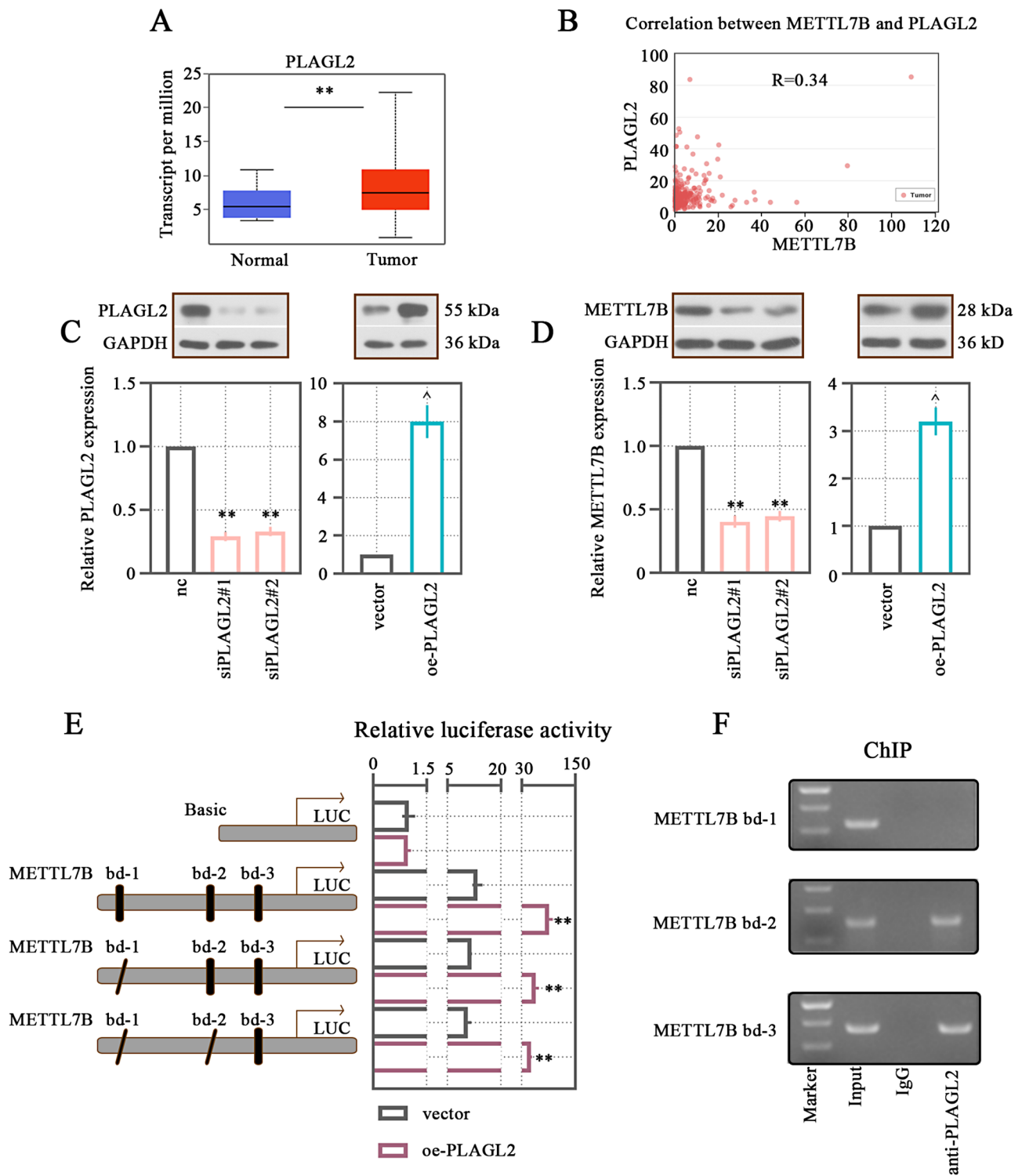


Fig. 6 Involvement of PLAGL2 in METTL7B transcriptional regulation. **A-B** Expression **(A)** of PLAGL2 and the correlation analysis **(B)** between PLAGL2 and METTL7B in bladder cancer from UALCAN database. Pearson Correlation Coefficient $R=0.34$, $P<0.05$. **C** Efficiencies of PLAGL2 knockdown or overexpression were validated by RT-qPCR in SW780 cells. $**P<0.01$ versus nc. $^{\wedge}P<0.05$ versus vector. **D** RT-qPCR and Western blot measurement of METTL7B expression in SW780 cells with PLAGL2 knockdown or overexpression. $**P<0.01$ versus nc. $^{\wedge}P<0.05$ versus vector. **E** METTL7B promoter activity upon PLAGL2 overexpression, as measure by dual luciferase method. $**P<0.01$ versus vector. **F** ChIP assay of PLAGL2 binding to METTL7B promoter. PLAGL2: PLAG1 Like Zinc Finger 2. METTL7B: methyltransferase-like 7B. UALCAN: University of Alabama at Birmingham Cancer Data Analysis Portal. ChIP: chromatin immunoprecipitation. nc: negative control. siPLAGL2#1/2: small interfering targeting PLAGL2. oe-PLAGL2: PLAGL2 overexpression plasmid. bd: potential binding domain. LUC: luciferase

to S phase transition. Moreover, CDKN2D was reported to inhibit CDK4 and CDK6 activity as well as to restrain G1/S transition [29]. Similar results of cell cycle-related gene expression upon METTL7B knockdown were reported by Li et al. [30], and Liu et al. [31]. These data supported the pro-proliferative effect of METTL7B, indicating a cancer promoting role for METTL7B on BC.

Ferroptosis, as one of the programmed cell death, plays an important role in the homeostatic mechanisms of organisms. The unique metabolism of cancer cells, their high ROS load, and cancer-specific mutations make some of these cells inherently susceptible to iron ion damage [32], including BC [33]. The family member METTL3 was reported to participate in ferroptosis process regulation [34]. In combination with the previous report for METTL7B on GPX4 expression [10], our work firstly revealed the function of METTL7B in ferroptosis. Erastin is a typical ferroptosis inducer. The experiment results showed that METTL7B silencing effectively aggravated Erastin-provoked lipid peroxidation and ferroptosis, manifested by lipid ROS, MDA, and iron content in BC cells. Additionally, these results were proved by mitochondrial morphological alternations observed by EM. Shrunken mitochondrial with reduced or vanished cristae and outer membrane rupture is the unique characteristic of ferroptosis [23], which was consistent with our EM results. All these results suggested the possible function of METTL7B on ferroptosis in BC. Xenotransplants also confirmed that knocking down METTL7B in SW780 cells decreased tumor growth; while, we noticed there was a mild decrease in tumor growth in METTL7B silencing upon Erastin induction, though there was no significance. It was unclear whether it was the inhibition of tumor proliferation beyond the constraints of the xenograft model, or perhaps the observation time point is too short to observe a time point where significant changes may occur. This also requires more thought and experimentally thinking.

The ferroptosis progress is under the regulation of ferroptosis regulator genes, which include suppressors and drivers of ferroptosis. In the past years, emerging evidence has reported that m⁶A regulated gene expression, and thus affect ferroptosis processes [35]. A recent work reveal unveils six possible ferroptosis-related prognostic genes for BC [24]. Three genes of interest were chosen for RT-qPCR examination upon METTL7B overexpression or silencing. Among them, ACSL3 with significant expression changes was chosen for further mechanism validation. ACSL3 belongs to the long-chain fatty ACSL family. Among this family, ACSL3 and ACSL4 were reported to function in ferroptosis. Concordant with ACSL4, ACSL3 is a suppressor of ferroptosis that regulate ferroptosis sensitivity which contributes to ferroptosis resistance in cancer cells [36–38]. Although the

precise function and target of METTL7B are inconclusive, it has recently been reported that METTL7B can participate in m⁶A modification as the RNA methyltransferase [10]. Our data showed that the m⁶A-methylated level of ACSL3 mRNA in BC cells upon METTL7B overexpression was significantly elevated. m⁶A methylation usually occurred in 3'-untranslated regions (3'-UTR) and then CDS as well as 5'-UTR region of mRNA [39]. It was experimentally confirmed that METTL7B promoted m⁶A modification on ACSL3 mRNA. Finally, a functional rescue experiment confirmed that METTL7B exerts functions in ferroptosis targeting ACSL3. The myriad roles of m⁶A modifications are largely dependent on downstream RNA binding proteins, known as m⁶A "readers", which preferentially recognize m⁶A-modified RNAs and then regulate mRNA processing [40, 41]. Thus, follow-up research with the identification of possible m⁶A readers will help to further understand the mechanism and it will be part of our future research.

Interestingly, we found that METTL7B is likely transcriptionally regulated by PLAGL1 like zinc finger 2 (PLAGL2). PLAGL2 contains seven C2H2 zinc finger domains on the N-terminal [42], which allows for DNA binding and activating transcription of specific genes [43]. The variety of cancers elaborates on the close relationship between PLAGL2 and tumor development [44, 45]. In BC, PLAGL2 was identified to be overexpressed and served as an independent predictor for survival [25]. PLAGL2 knockdown inhibited BC progression both in vivo and in vitro [46]. We observed that PLAGL2 regulated METTL7B directly by binding to -461~-451 and -262~-253 bp on METTL7B promoter transcriptional activity in BC cells, as ChIP results showed no binding at -1913~-1904 bp (bd-1 showing in Fig. 6F). It implicates that METTL7B was likely to be regulated by PLAGL2 in BC cells, thereby affecting downstream function. But, the exact molecular mechanism of PLAGL2 in BC and the underlying mechanism of the PLAGL2/METTL7B axis still need further investigation.

Conclusion

Our work uncovered the involvement of METTL7B in BC and upregulated METTL7B displayed the cancer promoting effect. Silencing METTL7B inhibited cell proliferation in BC cells. Mechanically, METTL7B promoted m⁶A modification on ACSL3 mRNA in BC cells, thereby inducing the ferroptosis process and regulating BC progression. Induction of ferroptosis is an effective therapeutic strategy. Researchers are exploring the induction of ferroptosis by small molecule compounds to enhance the sensitivity of chemotherapeutic drugs and thus improve the therapeutic effect of cancer, including BC [47]. The regulatory mechanism of ferroptosis is of great value in the clinical treatment of bladder cancer,

and future studies can focus on how to effectively induce ferroptosis and how to overcome the drug resistance of tumor cells.

Abbreviations

BC	Bladder cancer
NMIBC	Non-muscle invasive BC
MIBC	Muscle-invasive BC
METTL	Methyltransferase-like
SAM	S-adenosylmethionine
ROS	Reactive oxygen species
MDA	Malondialdehyde
IHC	Immunohistochemistry
RIPA	Radioimmune precipitation assay
PMSF	Phenylmethanesulfonyl fluoride
SDS-PAGE	Sodium dodecyl sulfate polyacrylamide gel electrophoresis
PVDF	Polyvinylidene fluoride
MeRIP	Methylated RNA immunoprecipitation
ANOVA	One-way analyses of variance
DEGs	Differentially expressed genes
CCLC	Cancer Cell Line Encyclopedia
3'-UTR	3'-untranslated regions
PLAGL2	PLAG1 like zinc finger 2

Supplementary Information

The online version contains supplementary material available at <https://doi.org/10.1186/s13062-025-00597-z>.

Supplementary Material 1: Supplementary figure 1. METTL7B knockdown inhibited protein expression of cell cycle-related genes. A) The protein expression of CCND1, CDK4, CDK6, and CDKN2D in SE780 and TCCSUP cells. CCND1: cyclin D1. CDKN2D: cyclin dependent kinase inhibitor 2D. CDK: cyclin dependent kinase. Con: control. shnc: negative control short hairpin RNA. sh1/2: short hairpin RNA 1/2 against METTL7B. nc: empty vector plasmid. oe: METTL7B overexpression plasmid.

Acknowledgements

None.

Author contributions

JNH designed the study and contributed to manuscript writing. JNH, CMD, XDS, ZKQ, and HZ performed the experiments. YJJ and TL performed statistics and revised the manuscript. XJM conducted project administration, carried out thorough supervision, and reviewed the manuscript. All authors read and approved the final manuscript.

Funding

This work was supported by the Scientific Research Project of the Education Department of Liaoning Province [grant numbers QN2019008]; the China Medical University's 2018 "Youth Support Program" (Natural Science) [grant number QGZ2018041]; and the China Medical University's Discipline Promotion Program.

Data availability

No datasets were generated or analysed during the current study.

Declarations

Ethics approval and consent to participate

The animal experiment was approved by the Ethics Committee of China Medical University.

Consent for publication

Not applicable.

Competing interests

The authors declare no competing interests.

Author details

¹Department of Surgical Oncology and Breast Surgery, The First Hospital of China Medical University, 155 North Nanjing Street, Heping District, Shenyang, Liaoning, China

²Department of Urology, The First Hospital of China Medical University, 155 North Nanjing Street, Heping District, Shenyang, Liaoning, China

³Institute of Urology, China Medical University, Shenyang, Liaoning, China

⁴Department of Urology, Shenyang Fifth People Hospital, Shenyang, Liaoning, China

⁵Institute of Urology, Benxi Central Hospital, 29 Shengli Road, Mingshan District, Benxi, Liaoning, China

Received: 9 August 2024 / Accepted: 6 January 2025

Published online: 20 January 2025

References

1. Antoni S, Ferlay J, Soerjomataram I, Znaor A, Jemal A, Bray F. Bladder Cancer incidence and mortality: A global overview and recent trends. *Eur Urol*. 2017;71(1).
2. Bray F, Ferlay J, Soerjomataram I, Siegel RL, Torre LA, Jemal A. Global cancer statistics 2018: GLOBOCAN estimates of incidence and mortality worldwide for 36 cancers in 185 countries. *CA Cancer J Clin*. 2018;68(6):394–424.
3. Patel VG, Oh WK, Galsky MD. Treatment of muscle-invasive and advanced bladder cancer in 2020. *CA Cancer J Clin*. 2020;70(5):404–23.
4. Stenzl A, Cowan NC, De Santis M, Jakse G, Kuczyk MA, Merseburger AS, et al. The updated EAU guidelines on muscle-invasive and metastatic bladder cancer. *Eur Urol*. 2009;55(4):815–25.
5. Abdollah F, Gandaglia G, Thuret R, Schmitges J, Tian Z, Jeldres C, et al. Incidence, survival and mortality rates of stage-specific bladder cancer in United States: a trend analysis. *Cancer Epidemiol*. 2013;37(3):219–25.
6. Petrossian TC, Clarke SG. Uncovering the human methyltransferase. *Mol Cell Proteomics*. 2011;10(1):M110000976.
7. Barbieri I, Kouzarides T. Role of RNA modifications in cancer. *2020;20(6):303–22*.
8. Thomas A, Klein MS, Stevens AP, Reinders Y, Hellerbrand C, Dettmer K, et al. Changes in the hepatic mitochondrial and membrane proteome in mice fed a non-alcoholic steatohepatitis inducing diet. *J Proteom*. 2013;80:107–22.
9. Nevalainen J, Skarp S, Savolainen ER, Rynänen M, Järvenpää J. Intra-uterine growth restriction and placental gene expression in severe preeclampsia, comparing early-onset and late-onset forms. *J Perinat Med*. 2017;45(7):869–77.
10. Song H, Liu D, Wang L, Liu K, Chen C, Wang L et al. Methyltransferase like 7B is a potential therapeutic target for reversing EGFR-TKIs resistance in lung adenocarcinoma. *2022;21(1):43*.
11. Jiang Z, Yin W, Zhu H, Tan J, Guo Y, Xin Z et al. METTL7B is a novel prognostic biomarker of lower-grade glioma based on pan-cancer analysis. *2021;21(1):383*.
12. McKinnon CM, Mellor H. The tumor suppressor RhoBTB1 controls golgi integrity and breast cancer cell invasion through METTL7B. *2017;17(1):145*.
13. Campeanu IJ, Jiang Y, Liu L, Pilecki M, Najor A, Cobani E, et al. Multi-omics integration of methyltransferase-like protein family reveals clinical outcomes and functional signatures in human cancer. *Sci Rep*. 2021;11(1):14784.
14. Dixon SJ, Lemberg KM, Lamprecht MR, Skouta R, Zaitsev EM, Gleason CE, et al. Ferroptosis: an iron-dependent form of nonapoptotic cell death. *Cell*. 2012;149(5):1060–72.
15. Lu B, Chen XB, Ying MD, He QJ, Cao J, Yang B. The role of ferroptosis in Cancer Development and Treatment Response. *Front Pharmacol*. 2017;8:992.
16. Hassannia B, Vandenabeele P, Vanden Berghe T. Targeting ferroptosis to Iron Out Cancer. *Cancer Cell*. 2019;35(6):830–49.
17. Sun Y, Berleth N, Wu W, Schlütermann D, Deitersen J, Stuhldreier F et al. Fin56-induced ferroptosis is supported by autophagy-mediated GPX4 degradation and functions synergistically with mTOR inhibition to kill bladder cancer cells. *2021;12(11):1028*.
18. Liu T, Jiang L, Tavana O, Gu W. The deubiquitylase OTUB1 mediates ferroptosis via stabilization of SLC7A11. *Cancer Res*. 2019;79(8):1913–24.
19. Geng Y, Zhou Y, Wu S, Hu Y, Lin K, Wang Y, et al. Sulforaphane Induced apoptosis via Promotion of Mitochondrial Fusion and ERK1/2-Mediated 26S proteasome degradation of Novel Pro-survival Bim and Upregulation of Bax in Human Non-small Cell Lung Cancer cells. *J Cancer*. 2017;8(13):2456–70.

20. Li T, Hu PS, Zuo Z, Lin JF, Li X, Wu QN et al. METTL3 facilitates tumor progression via an m(6)A-IGF2BP2-dependent mechanism in colorectal carcinoma. *2019*;18(1):112.
21. Chen C, He W, Huang J, Wang B, Li H, Cai Q, et al. LNMAT1 promotes lymphatic metastasis of bladder cancer via CCL2 dependent macrophage recruitment. *Nat Commun.* 2018;9(1):3826.
22. Delaunay S, Frye M. RNA modifications regulating cell fate in cancer. *2019*;21(5):552–9.
23. Liang C, Zhang X. Recent progress in Ferroptosis Inducers for Cancer Therapy. *2019*;31(51):e1904197.
24. Zhang S, Wang C, Xia W, Duan H, Qian S. Novel ferroptosis-related Multigene Prognostic models for patients with bladder Cancer. *2021*;14:8651–66.
25. Qu G, Xu Y, Wan SP, Yang G. Expression of PLAGL2 in bladder urothelial carcinoma and its relationship to lymph node metastasis and survival. *Sci Rep.* 2018;8(1):6044.
26. Wu CC, MacCoss MJ, Mardones G, Finnigan C, Mogelsvang S, Yates JR, et al. Organellar proteomics reveals golgi arginine dimethylation. *Mol Biol Cell.* 2004;15(6):2907–19. 3rd.
27. Liu GY, Luo Q, Xiong B, Pan C, Yin P, Liao HF, et al. Tissue array for Tp53, C-myc, CCND1 gene over-expression in different tumors. *World J Gastroenterol.* 2008;14(47):7199–207.
28. Witzel II, Koh LF, Perkins ND. Regulation of cyclin D1 gene expression. *Biochem Soc Trans.* 2010;38(Pt 1):217–22.
29. Sherr CJ, Roberts JM. CDK inhibitors: positive and negative regulators of G1-phase progression. *Genes Dev.* 1999;13(12):1501–12.
30. Li W, Xu S, Peng N, Zhang Z, He H, Chen R, et al. Downregulation of METTL7B inhibits proliferation of Human Clear Cell Renal Cancer cells in vivo and in Vitro. *Front Oncol.* 2021;11:634542.
31. Liu D, Li W, Zhong F, Yin J, Zhou W, Li S, et al. METTL7B is required for Cancer Cell Proliferation and Tumorigenesis in Non-small Cell Lung Cancer. *Front Pharmacol.* 2020;11:178.
32. Lei G, Zhuang L, Gan B. Targeting ferroptosis as a vulnerability in cancer. *2022*;22(7):381–96.
33. Zeng F, Lan Y, Wang N, Huang X, Zhou Q, Wang Y, Ferroptosis. A new therapeutic target for bladder cancer. *Front Pharmacol.* 2022;13:1043283.
34. Song Z, Jia G, Ma P, Cang S. Exosomal miR-4443 promotes cisplatin resistance in non-small cell lung carcinoma by regulating FSP1 m6A modification-mediated ferroptosis. *Life Sci.* 2021;276:119399.
35. Liu L, Li H, Hu D, Wang Y, Shao W, Zhong J et al. Insights into N6-methyladenosine and programmed cell death in cancer. *2022*;21(1):32.
36. Quan J, Bode AM, Luo X. ACSL family: the regulatory mechanisms and therapeutic implications in cancer. *Eur J Pharmacol.* 2021;909:174397.
37. Yang Y, Zhu T, Wang X, Xiong F, Hu Z, Qiao X et al. ACSL3 and ACSL4, distinct roles in Ferroptosis and cancers. *Cancers (Basel).* 2022;14(23).
38. Li D, Li Y. The interaction between ferroptosis and lipid metabolism in cancer. *Signal Transduct Target Therapy.* 2020;5(1):108.
39. Meyer KD, Saletore Y, Zumbo P, Elemento O, Mason CE, Jaffrey SR. Comprehensive analysis of mRNA methylation reveals enrichment in 3'UTRs and near stop codons. *Cell.* 2012;149(7):1635–46.
40. Wang X, Lu Z, Gomez A, Hon GC, Yue Y, Han D, et al. N6-methyladenosine-dependent regulation of messenger RNA stability. *Nature.* 2014;505(7481):117–20.
41. Wang X, Zhao BS, Roundtree IA, Lu Z, Han D, Ma H, et al. N(6)-methyladenosine modulates Messenger RNA translation efficiency. *Cell.* 2015;161(6):1388–99.
42. Wezensky SJ, Hanks TS, Wilkison MJ, Ammons MC, Siemsen DW, Gauss KA. Modulation of PLAGL2 transactivation by positive cofactor 2 (PC2), a component of the ARC/Mediator complex. *Gene.* 2010;452(1):22–34.
43. Soto A, Arce A, Vera MKK. Effect of the cation and the anion of an electrolyte on the solubility of DL-aminobutyric acid in aqueous solutions: measurement and modelling. *Biophys Chem.* 1998;73(1–2):77–83.
44. Yang YS, Yang MC, Weissler JC. Pleiomorphic adenoma gene-like 2 expression is associated with the development of lung adenocarcinoma and emphysema. *Lung cancer (Amsterdam Netherlands).* 2011;74(1):12–24.
45. Zheng H, Ying H, Wiedemeyer R, Yan H, Quayle SN, Ivanova EV, et al. PLAGL2 regulates wnt signaling to impede differentiation in neural stem cells and gliomas. *Cancer Cell.* 2010;17(5):497–509.
46. Chen H, Yang W, Li Y, Ji Z. PLAGL2 promotes bladder cancer progression via RACGAP1/RhoA GTPase/YAP1 signaling. *Cell Death Dis.* 2023;14(7):433.
47. Lin X, Ping J, Wen Y, Wu Y. The mechanism of ferroptosis and applications in Tumor Treatment. *Front Pharmacol.* 2020;11:1061.

Publisher's note

Springer Nature remains neutral with regard to jurisdictional claims in published maps and institutional affiliations.